Earth and Planetary Science Letters 601 (2023) 117892

Contents lists available at ScienceDirect

Earth and Planetary Science Letters

journal homepage: www.elsevier.com/locate/epsl

Low-degree melt metasomatic origin of heavy Fe isotope enrichment in the MORB mantle

Pengyuan Guo [a,b,*], Yaoling Niu [a,b,c,d], Shuo Chen [a,b], Meng Duan [a,b], Pu Sun [a,b], Yanhong Chen [d], Hongmei Gong [a,b], Xiaohong Wang [a,b]

[a] Key Laboratory of Marine Geology and Environment, Institute of Oceanology, Chinese Academy of Sciences, Qingdao 266071, China
[b] Laboratory for Marine Geology, Qingdao National Laboratory for Marine Science and Technology, Qingdao 266061, China
[c] Department of Earth Sciences, Durham University, Durham DH1 3LE, UK
[d] China University of Geosciences, Beijing 100083, China

ARTICLE INFO

Article history:
Received 10 May 2022
Received in revised form 19 October 2022
Accepted 28 October 2022
Available online 9 November 2022
Editor: R. Hickey-Vargas

Keywords:
mid-ocean ridge basalts
Fe isotope
upper mantle heterogeneity
low-degree melt metasomatism
Mid-Atlantic Ridge

ABSTRACT

Studies of mid-ocean ridge basalts (MORB) show a variable Fe isotope composition of the oceanic upper mantle. To test a recent hypothesis that heavy Fe isotope enrichment in the MORB mantle results from the same process of incompatible element enrichment, we conduct an Fe isotope study of well-characterized MORB samples from a magmatically robust segment (OH-1) of the Mid-Atlantic Ridge (MAR) at ~ 35°N. The data show large Fe isotope variation (δ^{56}Fe = +0.03 to +0.18‰) that correlates well with the abundances and ratios of more-to-less incompatible elements and with Sr-Nd-Hf isotopes. Our findings in support of the hypothesis can be detailed as follows: (1) the oceanic upper mantle has a heterogeneous Fe isotope composition on varying small spatial scales with isotopically heavy Fe (high-δ^{56}Fe) preferentially associated with pyroxenite lithologies; (2) such lithologies, which are also enriched in the progressively more incompatible elements, are of low-degree (low-F) melt metasomatic origin; (3) with all the conceivable processes considered, the low-F melt metasomatism takes place at the lithosphere-asthenosphere boundary (LAB) beneath ocean basins through crystallization of incipient (Low-F) melt in the seismic low velocity zone (LVZ) at the base of the growing oceanic lithosphere (i.e., LAB) over the Earth's history since the onset of plate tectonics, forming composite lithologies with geochemically enriched pyroxenite veins dispersed in the depleted peridotite matrix; (4) such mantle of composite lithology when transported to beneath the present-day ocean ridges will undergo decompression melting and produce MORB melts with geochemical trends of "melting-induced mixing" as observed at the MAR and global MORB; (5) we predict all this to be a globally common process and widespread.

1. Introduction

Analyses of mid-ocean ridge basalts (MORB) have shown that the oceanic upper mantle is compositionally heterogeneous on all scales in term of chemical elements and radiogenic Sr-Nd-Pb-Hf isotopes (e.g., Sun et al., 1979; Zindler et al., 1984; Mahoney et al., 1994; Salters and White, 1998). Such heterogeneity is often interpreted to indicate the MORB mantle containing dispersed materials of varying origin, including subducted seafloor materials, metasomatized deep portions of oceanic lithosphere, terrigenous sediments and continental lithosphere (McKenzie and O'Nions, 1995; Niu et al., 1996, 2002; Hofmann, 1997; White, 2015). Studies also show that MORB samples from ridges both away from and nearby mantle plumes have large Fe isotopic variation (δ^{56}Fe = +0.05 to +0.36‰; Fig. 1a and 2a) (Weyer and Ionov, 2007; Teng et al., 2013; Nebel et al., 2013; Chen et al., 2019; Sun et al., 2020; Gleeson et al., 2020; Richter et al., 2021), beyond explanation by processes of mantle melting from a uniform source (Weyer and Ionov, 2007; Dauphas et al., 2009; Williams and Bizimis, 2014) and magma evolution (Teng et al., 2008; Chen et al., 2019, 2021), indicating Fe isotope heterogeneity in the oceanic upper mantle (Sossi et al., 2016). A comprehensive study of abyssal peridotites further confirms the upper mantle Fe isotope heterogeneity (δ^{56}Fe = −0.08 to +0.12‰; Craddock et al., 2013). However, the origin of upper mantle Fe isotope heterogeneity remains enigmatic.

Because iron is the most abundant element of the earth by mass and is a major constituent of the mantle, it is fundamen-

* Corresponding author at: Institute of Oceanology, Chinese Academy of Sciences, 7 Nanhai Road, Qingdao, Shandong 266071, China.
E-mail address: guopy@qdio.ac.cn (P. Guo).

https://doi.org/10.1016/j.epsl.2022.117892

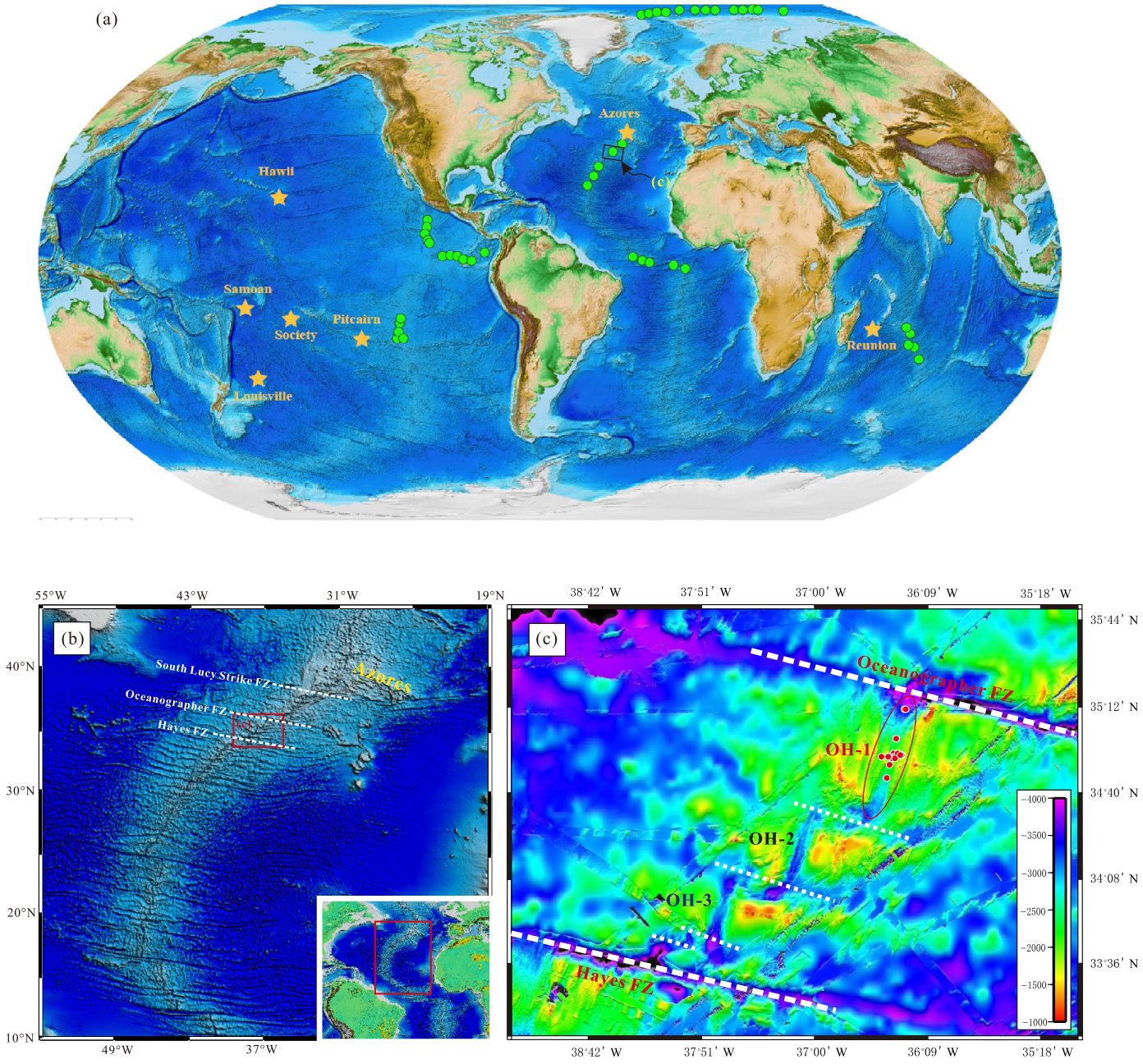

Fig. 1. (a) Global distribution of MORB (green circles) and OIB (orange stars) samples with Fe isotope data available; (b) Portion of the bathymetric map of the North Atlantic; (c) Detailed bathymetric map showing the Mid-Atlantic Ridge between the Oceanographer Fracture Zone (OFZ) and the Hayes Fracture Zone (HFZ) (data from NOAA bathymetric coverage), highlighting ridge segment OH-1 where new data are reported and discussed in detail in this paper in a global context. Sample locations are shown as solid red circles. (For interpretation of the colors in the figure(s), the reader is referred to the web version of this article.)

tal to understand the origin of mantle Fe isotope heterogeneity in the context of the chemical differentiation of the Earth. Our recent study on near-ridge seamounts flanking the East Pacific Rise (EPR) shows correlated variations of δ^{56}Fe values with the abundances of major elements, incompatible trace elements and radiogenic Sr-Nd-Pb-Hf isotopes, leading to the hypothesis that MORB mantle heavy Fe isotope (^{56,57}Fe vs. light ^{54}Fe) enrichment results from the same process of incompatible element enrichment associated with low-degree melt mantle metasomatism in Earth's history (Sun et al., 2020).

The above finding on EPR seamount lavas (Sun et al., 2020) is important, but whether it is a general MORB mantle feature of global significance requires testing. We choose to test this hypothesis by studying a well-characterized MORB suite from ridge segment OH-1 of the slow-spreading mid-Atlantic Ridge (MAR) at ∼ 35°N (Fig. 1) for the following reasons: (1) Compared to the fast-spreading EPR in an old ocean basin, the slow-spreading MAR developed in the relatively younger ocean basin with passive continental margins is expected to have different sub-ridge mantle source and source histories; (2) Ridge segment OH-1 of the MAR has large MORB compositional variation dominated by samples with elevated abundances of incompatible elements (e.g., $[La/Sm]_N = 0.56\text{-}2.99$; Niu et al., 2001) and enriched Sr-Nd-Hf isotopes (Guo et al., 2021), illustrating a large amplitude of source compositional variation with the enriched component best understood as lithologies of low-degree melt metasomatic origin dispersed in the refractory peridotitic matrix; (3) Compared to other ridge segments of the region, OH-1 is magmatically robust with

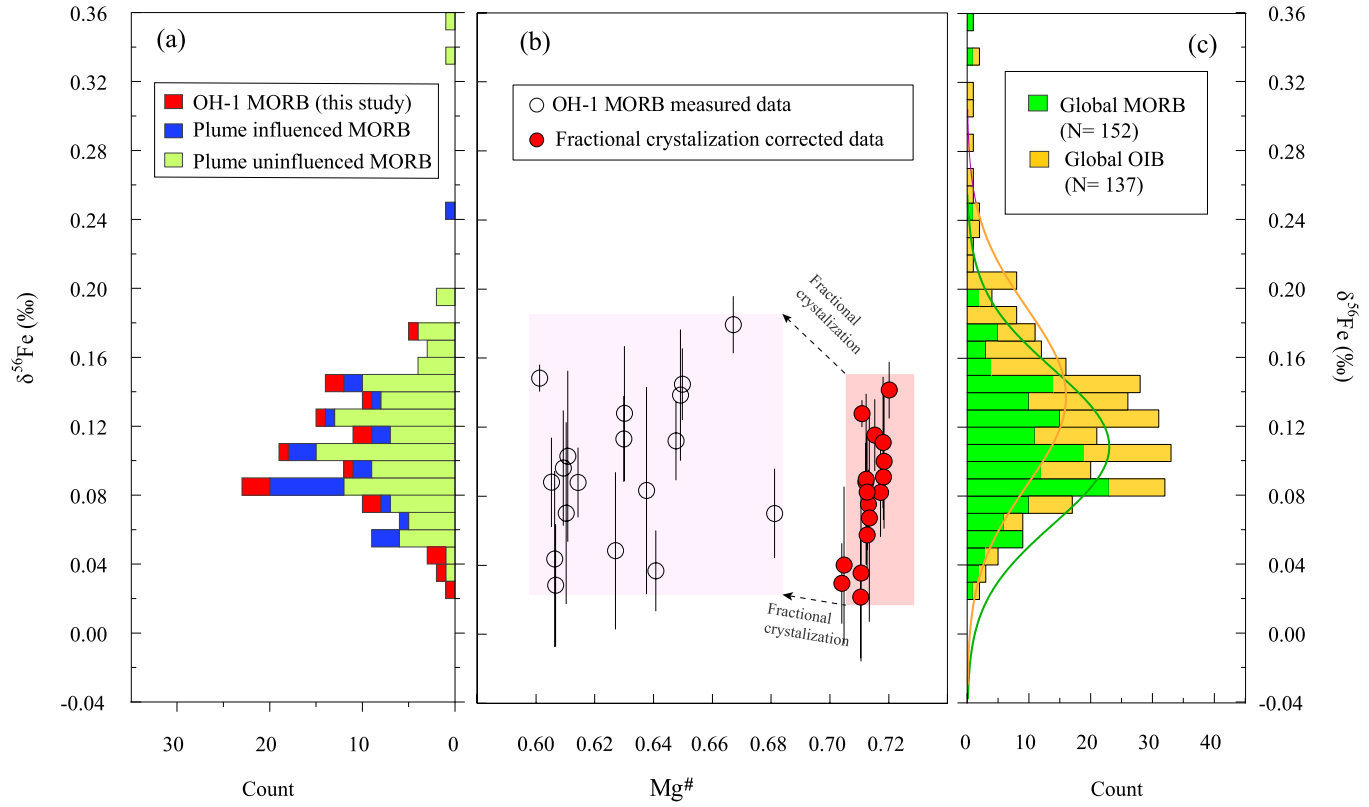

Fig. 2. (a) Histogram of δ^{56}Fe of OH-1 MORB lavas, compared with the available global MORB data from ridges far from hotspots (Weyer and Ionov, 2007; Teng et al., 2013; Nebel et al., 2013; Chen et al., 2019; Sun et al., 2020; Richter et al., 2021) and ridges influenced by mantle plumes (Gleeson et al., 2020); (b) δ^{56}Fe vs. Mg$^{\#}$ diagram for OH-1 MORB lavas. (c) Histogram of so-far available global MORB δ^{56}Fe data to show remarkable similarity to those of OIB in terms of Fe isotope variations range. The orange and green curves are normal distribution of global OIB and MORB, respectively.

a central topographic high and a large negative mantle Bouguer anomaly, consistent with greater extent of mantle melting of an enriched (easily melted) mantle source to produce thicker magmatic crust, much more so than ridge segments north of the Oceanographer Transform towards the Azores Platform, demonstrating that the development of OH-1 is unrelated to the Azores mantle plume (Niu et al., 2001). Hence, ridge segment OH-1 of the MAR is a prime test-ground for testing the low-degree melt metasomatism origin for isotopically heavy Fe enrichment in the global MORB mantle.

2. Samples and method

A total of 18 OH-1 MORB samples are analyzed in this study. Details of these samples have been reported (Bideau et al., 1998). Major and trace element concentrations and Sr-Nd-Hf isotopic compositions have also been reported (Niu et al., 2001; Guo et al., 2021). Iron isotope analysis is done in the Laboratory of Ocean Lithosphere and Mantle Dynamics, Institute of Oceanology, Chinese Academy of Sciences. About 5 mg (powder or glass fragments) of each dried sample is weighted for Fe isotope analysis. The sample dissolution and digestion follow Chen et al. (2017). After repeated re-flux using aqua regia to obtain full digestion, each sample is finally dissolved in 1 ml 9N HCl ready for chromatographic separation for Fe. Iron is purified using 1 ml anion-exchange resin (Bio-Rad AG MP-1M 200-400 mesh) conditioned with 9N HCl, following Gong et al. (2020). Matrix elements are removed by washing with 5 ml 9N HCl and 5 ml 6N HCl. Iron is eluted using 1.5 ml 1N HCl. The eluted Fe solutions are analyzed using ICP-OES to ensure purity and full recovery. Prior to measurements, Fe solutions are diluted to 14 ppm, and 19.6 ppm of GSB Ni standard (an ultrapure single elemental standard solution from the China Iron and Steel Research Institute) is added as an internal mass bias monitor to each diluted sample (Ni:Fe = 1.4:1). The isotope analysis is done using a Nu Plasma II Multi-Collector Inductively Coupled Plasma Mass Spectrometry (MC-ICP-MS) at condition of wet plasma at pseudo-high-resolution mode with Mass Resolution ≥ 7500. ^{60}Ni/^{58}Ni is used to monitor and correct for the instrumental mass fractionation. During analysis, every sample was bracketed with 14 ppm GSB Fe standard solution that is also doped with the GSB Ni solution with Ni:Fe of 1.4:1 (Gong et al., 2020). Our data are reported in per mil relative to IRMM014 ($\delta^{57}Fe_{IRMM014} = \delta^{57}Fe_{GSB} + 1.073$; $\delta^{56}Fe_{IRMM014} = \delta^{56}Fe_{GSB} + 0.729$; He et al., 2015). Every sample solution is repeatedly analyzed three to six times, with the average δ^{56}Fe and δ^{57}Fe values of each sample given in Table 1. The long-term δ^{56}Fe of an in-house standard Alfa Fe solution is 0.05‰ (2SD). The whole procedural Fe blank is < 33 ng, which is negligible for the minimum amounts (~255 μg) of Fe processed. The Fe isotopic analyses of the USGS reference materials (Table 1) run together with our samples agree well with the reported values (GeoREM, http://georem.mpch-mainz.gwdg.de/).

3. Results

The measured Fe isotope data of the OH-1 MORB lavas are given in Table 1 and plot as a function of Mg$^{\#}$ (Mg$^{\#}$ = Mg/[Mg+Fe^{2+}]; Fig. 2b). The studied 18 samples show large δ^{56}Fe variation (+0.03 to +0.18‰ with an average of +0.10 ± 0.08‰, 2SD; Fig. 2a), reflecting a rather large mantle Fe isotope variability on such a ridge segment scale (Fig. 1c). In order to rule out the effect of fractional crystallization, we corrected the Fe isotopes to a melt with Mg$^{\#}$ = 0.72 in equilibrium with mantle olivine (Fig. 2b) following Chen et al. (2021) (see Supplementary materials). The correction lowers the δ^{56}Fe values only by 0.01-0.03‰ (within analytical error; Gong

Table 1
Fe isotope analysis results on MORB from Mid-Atlantic Ridge at ~35°N.

Sample	Lat. N	Long. W.	$[La/Sm]_N$	$Mg^{\#}$	$\delta^{56}Fe$	2SD	$\delta^{57}Fe$	2SD	N
OT01-04	34.894	−36.428	0.94	0.61	0.07	0.05	0.07	0.07	4
OT01-07	34.895	−36.436	0.98	0.61	0.04	0.05	0.13	0.04	4
OT02-09	34.867	−36.438	1	0.61	0.03	0.04	0.05	0.06	4
OT02-11	34.860	−36.433	2.67	0.65	0.14	0.02	0.24	0.08	4
OT03-02	34.823	−36.468	1.77	0.6	0.15	0.01	0.26	0.05	3
OT05-02	34.890	−36.414	1.5	0.61	0.09	0.02	0.13	0.06	4
OT05-08	34.885	−36.388	2.39	0.65	0.11	0.02	0.18	0.02	4
OT05-13	34.878	−36.376	2.89	0.67	0.18	0.02	0.24	0.04	4
OT06-01	34.880	−36.380	2.99	0.63	0.11	0.02	0.16	0.05	4
OT16-01	34.872	−36.531	1.09	0.63	0.13	0.04	0.19	0.06	4
OT16-11	34.872	−36.476	0.79	0.64	0.04	0.02	0.1	0.06	4
OT17-06	34.977	−36.420	1.97	0.61	0.09	0.03	0.14	0.06	4
OT17-09	34.980	−36.419	1.44	0.61	0.1	0.05	0.12	0.08	5
OT17-09R					0.1	0.03	0.13	0.07	4
OT18-04	34.865	−36.450	2.78	0.65	0.14	0.04	0.2	0.07	5
OT18-11	34.873	−36.468	0.69	0.63	0.05	0.05	0.11	0.09	4
OT19-04	34.738	−36.492	0.56	0.68	0.07	0.03	0.11	0.06	3
OT20-05	35.165	−36.361	1.28	0.61	0.1	0.03	0.16	0.06	6
OT20-06	35.159	−36.346	1.11	0.64	0.08	0.06	0.13	0.06	6
BCR-2					0.08	0.05	0.09	0.08	12
AGV-2					0.12	0.01	0.13	0.05	4
GSP-2					0.16	0.02	0.18	0.07	4
W-2a					0.04	0.02	0.06	0.06	5

Note: The three samples OT16-11, OT18-11, OT19-04 are explained as having different mantle source and source history with other OH-1 samples (Guo et al., 2021). Therefore, we do not include these three samples in the co-variation plots.

et al., 2020) without affecting the intrinsic feature of the data as manifested by the significant correlation ($R^2 = 0.986$, N = 18) between the measured $\delta^{56}Fe$ and the corrected $\delta^{56}Fe_{corr}$ (Fig. 3a), indicating that magma differentiation has a limited effect on OH-1 lava $\delta^{56}Fe$ (see Fig. 3b-d). Nevertheless, we use $\delta^{56}Fe_{corr}$ values in the following discussion. What is striking is the statistically significant correlations ($R^2 \geq 0.42$; $N = 15$) of $\delta^{56}Fe_{corr}$ with the abundances (e.g., K_2O, Ba, La) and ratios of more-to-less incompatible elements (e.g., $[La/Sm]_N$, K_2O/TiO_2, Zr/Y) (Fig. 4), and with Sr-Nd-Hf isotopes (Fig. 5). Note that three samples (OT16-11, OT18-11 and OT19-04) show distinct trends in elemental-isotope diagrams (see Fig. 5 in Guo et al., 2021), being consistent with different mantle source and source history (Guo et al., 2021). Therefore, we do not include these three samples in the following discussion.

4. Discussion

4.1. Mantle source inheritance of the Fe isotope variation in the OH-1 MORB

Apart from the mantle source heterogeneity, several processes could potentially contribute to the observed $\delta^{56}Fe$ variation in the OH-1 lavas, including seawater alteration (e.g., Rouxel et al., 2003), fractional crystallization (Teng et al., 2008; Chen et al., 2019, 2021) and partial melting (Weyer and Ionov, 2007; Dauphas et al., 2009; Williams and Bizimis, 2014). Thus, it is necessary to evaluate the influence of these processes before discussing the mantle source Fe isotope heterogeneity. The effect of seawater can be ruled out because it will not cause the observed correlations of Fe isotopes with $[La/Sm]_N$, $^{143}Nd/^{144}Nd$ and $^{176}Hf/^{177}Hf$ (Figs. 4 and 5). Second, the OH-1 lavas experienced limited magma evolution with $Mg^{\#} = 0.60$ - 0.68 (Niu et al., 2001) and there is no $\delta^{56}Fe$-$Mg^{\#}$ correlation (Fig. 2b), thus liquidus mineral crystallization is unlikely the cause of the large $\delta^{56}Fe$ variation. Nevertheless, to ensure that our results are not influenced by fractional differentiation, we still corrected for the possible effect of fractional crystallization by back tracking $\delta^{56}Fe$ values to the expected primary melt with $Mg^{\#} = 0.72$ (see Supplementary materials). As noted above, fractional crystallization has limited effect without affecting the intrinsic feature of the OH-1 MORB $\delta^{56}Fe$ data as demonstrated by the correlated variations of $\delta^{56}Fe$ with incompatible element abundances and Sr-Nd-Hf isotopes (Fig. 3 and 5). Third, previous studies show that varying extent of MORB mantle melting (~10 to 20%; Niu, 1997) of a uniform source would produce no more than 0.03‰ $\delta^{56}Fe$ differences in the melts (Dauphas et al., 2009; Williams and Bizimis, 2014; Gleeson et al., 2020; Soderman et al., 2021), which is within analytical error (Gong et al., 2020) and thus is negligible relative to the 0.15‰ $\delta^{56}Fe$ variation range of the OH-1 lavas. In addition, process such as magma mixing in crustal magma chambers (Niu, 1997) could change the composition of the magmas, but this 'homogenization' effect on the erupted melts would reduce the $\delta^{56}Fe$ variability, yet retention of the correlated variations of $\delta^{56}Fe$ with abundances and ratios of incompatible elements and radiogenic isotopes in the OH-1 lavas (Figs. 4 and 5) indicates that this effect is also negligible. Therefore, the $\delta^{56}Fe$ variation and its significant correlations with the abundances and ratios of incompatible elements and with radiogenic isotopes of the OH-1 lavas (Figs. 4 and 5) reflect clear mantle source inheritance beneath this part of the MAR.

4.2. Low-degree melt metasomatic origin of heavy Fe isotope enrichment in the OH-1 MORB mantle

Because low-degree melting can effectively fractionate elements of varying incompatibilities, especially between elements with small or subtle incompatibility difference, low-degree melt metasomatism has long been speculated to cause localized mantle enrichment that later participated in mantle melting for incompatible element enriched basalts such as enriched mid-ocean ridge basalts (E-MORB), ocean island basalts (OIB) and alkali basalts in various settings (e.g., Sun and Hanson, 1975; Halliday et al., 1995; Niu et al., 2002; Niu and O'Hara, 2003; Niu and Green, 2018; Guo et al., 2016; Sun et al., 2021). It is also well understood that such low-degree melt metasomatism most likely takes place at the very base of the thickening oceanic lithosphere (Niu and Green, 2018), i.e., the lithosphere-asthenosphere boundary (LAB), where incipient melt (metasomatic agent) of asthenosphere (seismic low velocity zone or LVZ) origin solidifies as veins/veinlets of amphibole-(phlogopite)-clinopyroxene-garnet assemblage of low solidus in the predominantly refractory peridotite ambience (Fig. 6a). The

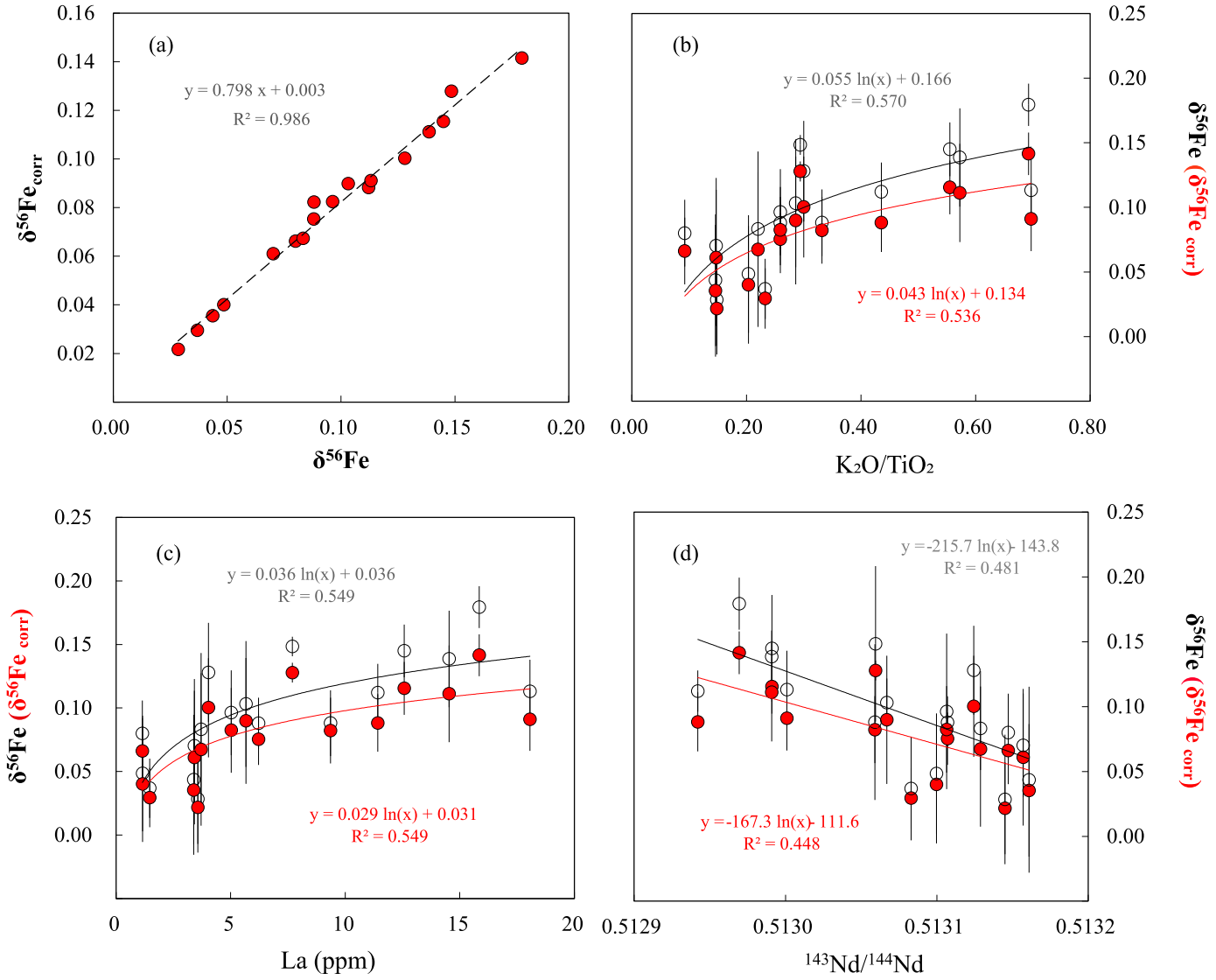

Fig. 3. Comparison between observed δ^{56}Fe and fractional crystallization corrected-δ^{56}Fe (i.e., $\delta^{56}Fe_{corr}$) values for the OH-1 MORB samples. The corrected $\delta^{56}Fe_{corr}$ values show a systematic difference from the observed δ^{56}Fe (R^2 = 0.986), but the absolute difference is small and the effect of fractional crystallization only elevates δ^{56}Fe by 0.01 to 0.03‰, well within the analytical error (0.05‰; Gong et al., 2020). Also shown are the $\delta^{56}Fe(\delta^{56}Fe_{corr})$-$K_2O/TiO_2$, $\delta^{56}Fe(\delta^{56}Fe_{corr})$-La, and $\delta^{56}Fe(\delta^{56}Fe_{corr})$-$^{143}Nd/^{144}Nd$ diagrams to illustrate that the correlations of δ^{56}Fe with the abundances and ratios of the incompatible elements, and radiogenic isotopes in the OH-1 lavas reflect their primary magma characters, which are mainly inherited from their heterogeneous mantle source with the effect of magma differentiation being negligible.

veins/veinlets of low-F melt metasomatic origin are understood to be enriched in incompatible elements (Fig. 4a-c; e.g., K_2O, Ba, La) and more so in the progressively more incompatible elements as we observe (Fig. 4d-f; e.g., higher ratios of $[La/Sm]_N$, K_2O/TiO_2, Zr/Y), which affirms the hypothesis (Sun et al., 2020) that heavy Fe isotope (high $\delta^{56,57}$Fe) enrichment is of the same low-F melt metasomatic origin for incompatible element enrichment (Fig. 4, Fig. S1; Guo et al., 2021), which is further detailed below. Note that while Fe isotopes and incompatible trace elements fractionate during low-degree partial melting, radiogenic isotopes require time integrated high Rb/Sr, low Sm/Nd and low Lu/Hf ratios, respectively. Thus, the positive correlation of δ^{56}Fe with $^{87}Sr/^{86}Sr$ and negative correlation with $^{143}Nd/^{144}Nd$ and $^{176}Hf/^{177}Hf$ (Fig. 5) indicate an ancient formation of metasomatically enriched mantle.

Fragments of such ancient lithosphere with vein lithologies of metasomatic origin (Fig. 6a) are expected to be widespread in the mantle and will, when transported to beneath ocean ridges, undergo decompression melting, producing compositionally variable MORB melts with correlated variations (Fig. 6b). However, we should note that the original metasomatic vein lithologies must have been "metamorphosed" to the more stable garnet pyroxenites before transported to the MORB mantle sources because of mantle circulation. We thus assume this 'metamorphism' must have been a 'closed system' process and does not modify the geochemical (including Fe isotope) signature of metasomatic veins/veinlets. This assumption is valid as it takes place under sub-solidus conditions in the mantle involving only P-T-variation controlled phase transformation that differs from the familiar crustal and subduction-zone metamorphism where fluids play important roles in mobilizing many chemical elements and their isotopes. It follows that basalts formed in all tectonic settings on Earth are expected to inherit heavy Fe isotope enrichment if their sources contain geochemically enriched lithologies of low-F melt metasomatic origin although such signature could be camouflaged by other factors such as subduction zone processes and subducted materials of varying origin in Earth's histories, but requiring further test of this hypothesis in future global studies.

With all the conceivable scenarios considered, we maintain that low-F melt metasomatism most likely takes place at the LAB beneath ocean basins (e.g., Niu and O'Hara, 2003; Niu and Green,

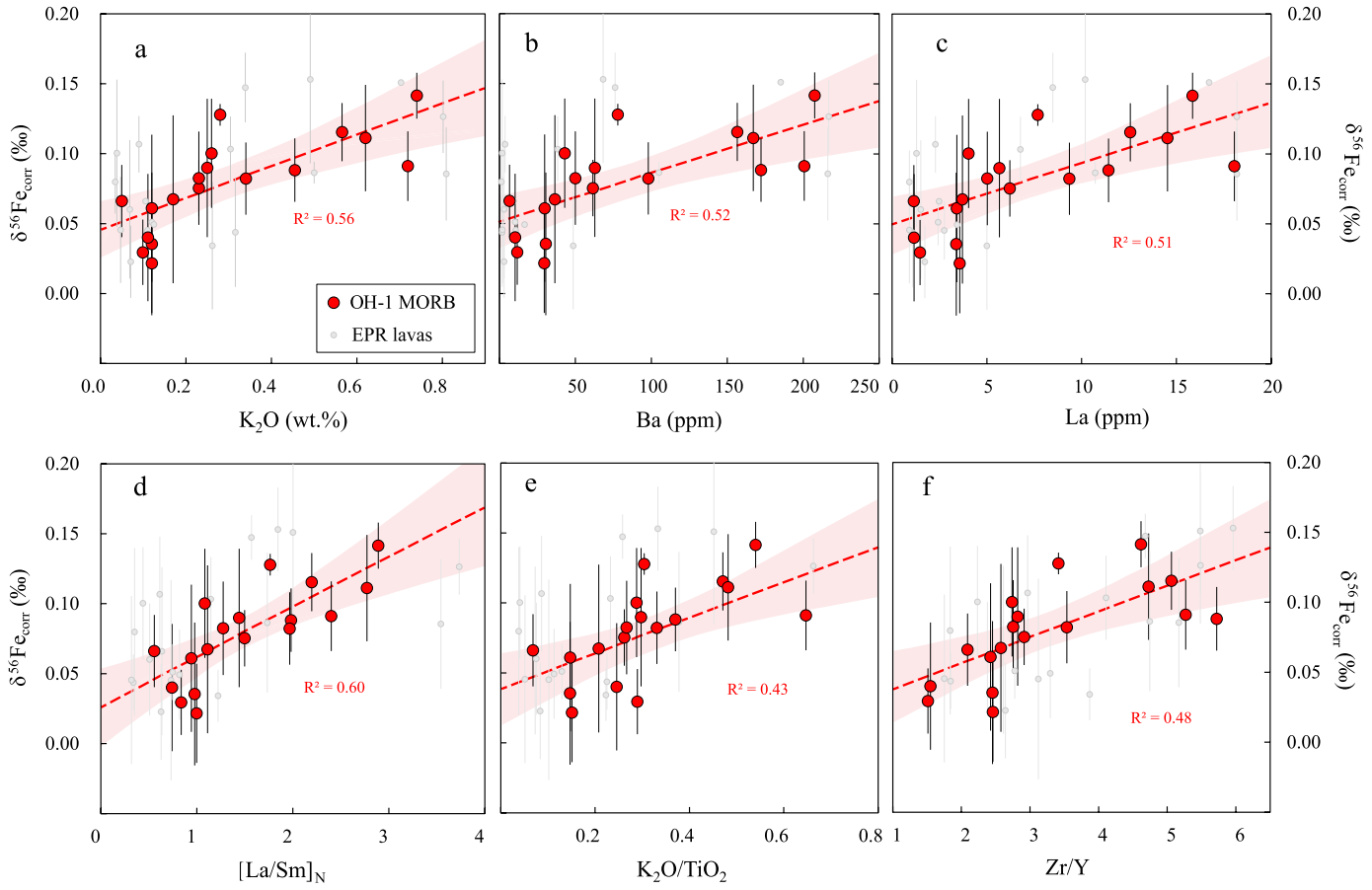

Fig. 4. $\delta^{56}Fe_{corr}$ variation with the abundances and ratios of incompatible elements in the OH-1 MORB lavas. a-c, $\delta^{56}Fe$ variation as a function of K_2O, Ba, La; d-f, $\delta^{56}Fe$ variation as a function of $[La/Sm]_N$ (primitive mantle normalized following Sun and McDonough, 1989), K_2O/TiO_2, Zr/Y. We also plot the East Pacific Rise (EPR) seamount lavas (gray circles; Sun et al., 2020) for comparison. Error bars of $\delta^{56}Fe$ on individual data points are ±2SD. The best-fit linear regression lines at 95% confidence intervals with R^2 values are given for the OH-1 lavas.

2018) at present and in Earth's history since the onset of plate tectonics. Metasomatism in the mantle wedge above subduction zones proposed by some authors (Ferry and Dipple, 1991; Donnelly et al., 2004; Bebout, 2013) is possible but is less likely because of the high-degree flux melting and also because there is no evidence of 'subduction-zone magma signatures' (e.g., depletion in Nb, Ta, Ti) in enriched basalts with lithologies of low-F metasomatic origin. The mature cratonic LAB is also unlikely because of lacking oceanic type LVZ with incipient low-F melt for metasomatism. The continental LAB beneath regions of lithosphere thinning as the result of basal hydration weakening is possible for such a low-F melt metasomatism, because the lithosphere thinning is the very process of oceanic type LVZ development with incipient low-F melt present as exampled in eastern continental China (Niu, 2014; Sun et al., 2021).

4.3. The concept of melting-induced mixing of lithologically heterogeneous mantle source

It is conceptually important to note that the observed correlations (Figs. 4–5) are geochemical mixing trends between melts with varying less contributions of such vein lithologies and varying greater contributions of the refractory peridotite matrix. We would not see the mixing trends (Figs. 4–5) if the enriched lithologies are uniformly distributed in the refractory peridotite matrix and if the overall extent of melting is the same recorded by each of these samples. These trends are thus melting-induced mixing of lithologically composite mantle source, resulting from (1) varying extent melting of such composite source, or (2) similar extent melting of the composite mantle containing variable proportions of the two lithologies (Niu et al., 2002; Niu and Hékinian, 2004). To illustrate this concept, we model the melting-induced mixing of the two distinct lithologies by using a depleted/refractory peridotite as the mantle matrix (Workman and Hart, 2005) and the average of seven garnet pyroxenites (Zhao et al., 2017) as the enriched lithologies of low-F melt metasomatic origin (see modelling details in Supplementary materials). The modelling demonstrates that the OH-1 lavas can be produced by ~10% melting (e.g., Niu et al., 2001) with ~0 to 70% pyroxenite contribution or 30 to 100% contribution of peridotitic mantle matrix (Fig. 6c)

4.4. A possible mechanism of Fe isotope fractionation during low-F melt mantle metasomatism

Isotopically heavy Fe (i.e., $^{56,57}Fe$ vs. ^{54}Fe) enrichment in the process of low-F melt metasomatism in causing upper mantle compositional heterogeneity is irrefutably clear in the OH-1 MORB samples (Figs. 3–5) and in the EPR seamount lavas (Sun et al., 2020). But why low-F melt prefers to concentrate heavy Fe isotope (hence, imparting the heavy Fe signature in the resulting pyroxenite lithologies) needs understanding. The data require heavy Fe isotope behaving more as an 'incompatible element'. We cannot rule out the possibility that heavy isotopes (e.g., $^{56,57}Fe$) tend to behave 'more incompatibly' than light isotope (e.g., ^{54}Fe) independent of a redox change during low-F melt processes, which might also be the case such as Mo (Chen et al., 2022), which is yet to be experimentally tested. Alternatively, the apparently more incompatible behavior of heavier Fe isotopes can be understood in terms

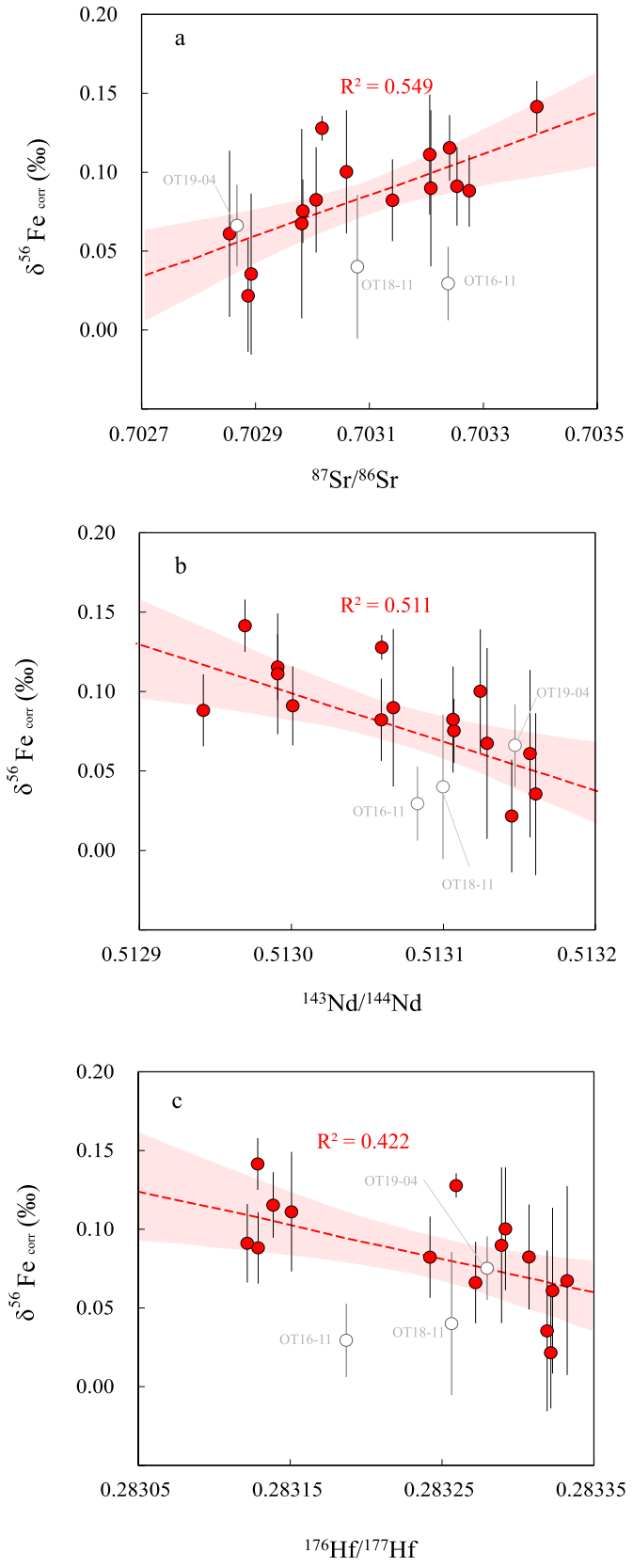

Fig. 5. $\delta^{56}Fe_{corr}$ variation as a function of $^{87}Sr/^{86}Sr$, $^{143}Nd/^{144}Nd$ and $^{176}Hf/^{177}Hf$ in the OH-1 MORB lavas. Error bars of $\delta^{56}Fe$ on individual data points are ±2SD. The best-fit linear regression lines at 95% confidence intervals with R^2 values are given. Note that samples OT16-11, OT18-11 and OT19-04 are considered to be originated from a different mantle source (Guo et al., 2021), we, thus, did not include these three samples in the R calculation and in the discussion.

of the differential behavior between Fe^{3+} and Fe^{2+}. Fe^{3+} is shown to be more incompatible than Fe^{2+} during mantle melting (Canil et al., 1994; Dauphas et al., 2009; O'Neill et al., 2018) and it is also argued that the heavier $^{56,57}Fe$ (vs. ^{54}Fe) prefers to form Fe^{3+}-O (vs. Fe^{2+}-O) bonds in silicate melts (Dauphas et al., 2014; Sossi and O'Neill, 2017). Such $^{56,57}Fe$-Fe^{3+} affinity can thus explain the coupling of high-$\delta^{56}Fe$ with the enrichment of progressively more incompatible elements and Sr-Nd-Hf isotopes in the OH-1 MORB samples as well as in the EPR seamount lavas (Sun et al., 2020). We prefer to accept the latter reasoning at present but also note the necessity for testing the former possibility. In this case, one would expect high Fe^{3+}/Fe^{2+} in the incompatible element enriched lavas with high $\delta^{56}Fe$, which indeed seems to be the case in the Cenozoic alkali basalts from eastern continental China (He et al., 2019). But we emphasize that our observed Fe isotope fractionation in the MORB mantle must have occurred in earth's history (>1 Ga) because of the correlations of $\delta^{56}Fe$ with radiogenic isotopes and we cannot rule out subsequent Fe^{3+}/Fe^{2+} changes as a result of subsolidus redox reactions on scales within the enriched lithologies. Therefore, lacking any $\delta^{56}Fe$ - Fe^{3+}/Fe^{2+} correlation in MORB samples of ancient low-F melt enrichment will not negate the above interpretation. These uncertainties will not affect our conclusions here but need consideration in revealing actual mechanisms of Fe isotope fractionation.

4.5. Global significance of heavy Fe isotope enrichment as a result of low-F melt mantle metasomatism

By using MORB samples from ridge segment OH-1 of the MAR, we have successfully verified the hypothesis based on near-EPR seamount lavas that heavy Fe isotope enrichment in the MORB mantle results from the same process of incompatible element enrichment as a consequence of low-F melt mantle metasomatism (Sun et al., 2020). The Pacific is an ancient ocean with a long spreading-subduction history whereas the Atlantic is a young ocean basin with passive continental margins, suggesting that MAR and EPR mantle sources and source histories may be different. However, we observe the same geochemical systematics of MORB mantle sources, including correlated variations of heavy Fe enrichment, incompatible element enrichment and Sr-Nd-Hf radiogenic isotopes (Figs. 4 and 5; and also see Sun et al., 2020). These observations are informative that regardless of the origin, history and seafloor spreading rate variation of different ocean basins, the oceanic upper mantle is globally similarly heterogeneous with lithologies (e.g., pyroxenite veins/veinlets) of low-F melt mantle metasomatic origin randomly dispersed in the predominantly peridotite matrix (Niu and Hékinian, 2004). We can therefore hypothesize that heavy Fe isotope enrichment as the result of low-F melt metasomatism is a global MORB mantle compositional property (also see below).

To better appreciate the global significance of low-F melt metasomatism inducing upper mantle heavy Fe isotope enrichment, we compiled the available Fe isotope data of global MORB. We excluded the data on samples with $Mg^{\#} < 0.4$ and $Mg^{\#} > 0.72$ because these highly evolved samples or samples with $Mg^{\#} > 0.72$ do not genuinely reflect their mantle source Fe isotope compositions, but the modified by liquidus mineral separation or accumulation (Chen et al., 2019, 2021). The Fe isotope data of the remaining MORB samples were then corrected for the fractional crystallization effect (see details in Supplementary). Similar to OH-1 MORB lavas, the global MORB also display broad correlations of $\delta^{56}Fe_{corr}$ with the familiar mantle enrichment proxies, such as $[La/Sm]_N$, K_2O/Ti_2O, Nb/Y and Zr/Y (Fig. 7). These first order systematic Fe isotope variations in the global MORB dataset reflect a clear melting-induced mixing of the lithologically heterogenous mantle beneath ocean ridges discussed above (e.g., Niu et al., 2002; Sun

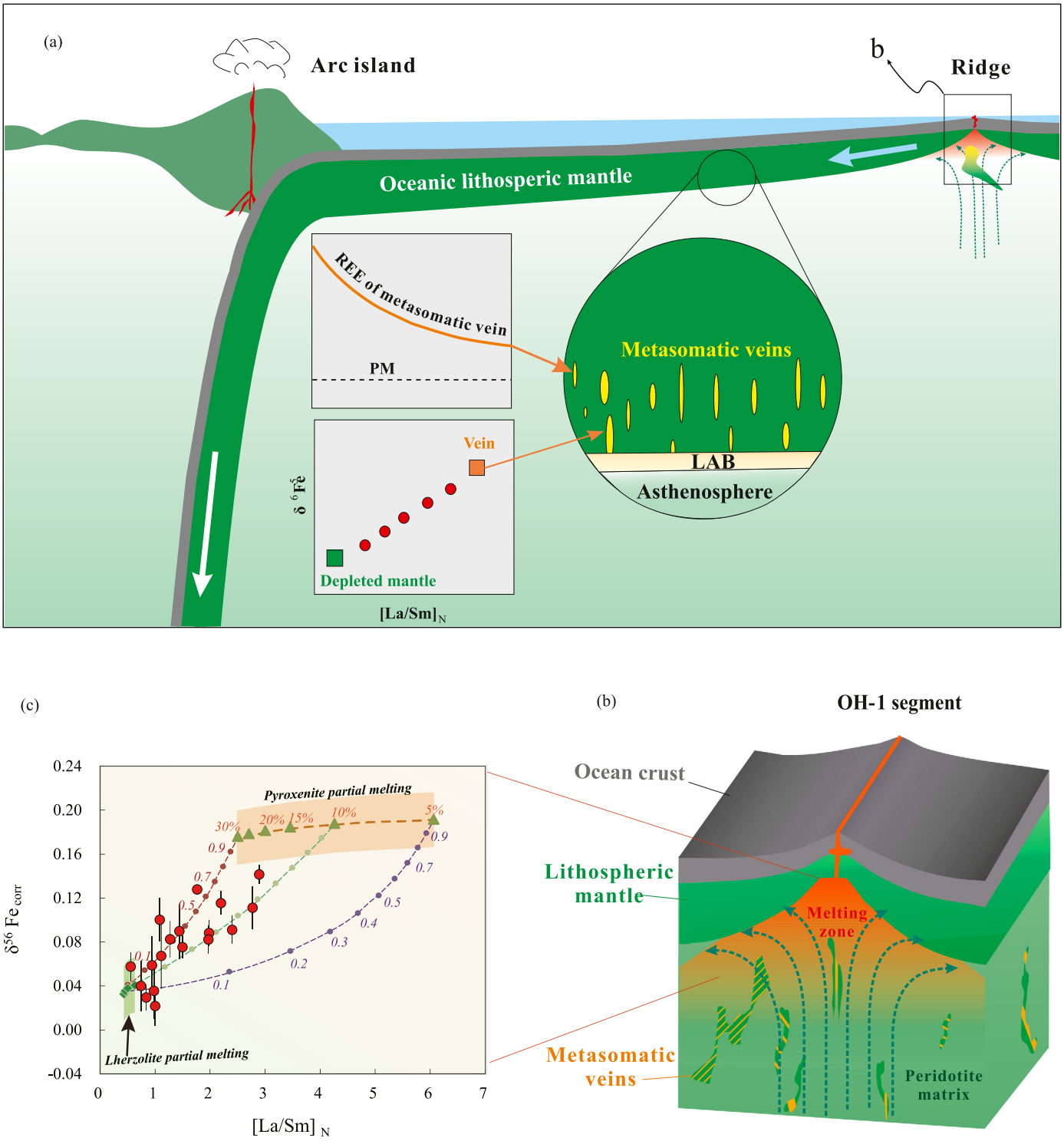

Fig. 6. Schematic illustrations on the origin of the Fe isotope systematics of the OH-1 MORB. (a) Cartoon shows the development of compositionally enriched pyroxenite veins/veinlets of metasomatic origin and lithospheric mantle recycling (modified from Niu et al., 2002). Incipient melt (i.e., low-degree melt) prevailing in the asthenosphere beneath ocean basins (Niu and Green, 2018) will precipitate geochemically enriched lithologies (e.g., pyroxenite veins/veinlets) at the base of the growing/thickening oceanic lithospheric mantle dominated by peridotites, forming composite lithologies in the deep portions of the oceanic lithosphere. Such vein/veinlet (yellow lenses) lithologies, relative to the peridotite matrix (green background), are enriched in incompatible elements with high δ^{56}Fe as indicated using the REE pattern and an orange square in the δ^{56}Fe-$[La/Sm]_N$ plot; (b) The geochemically enriched lithospheric mantle lithologies, whether subducted in the deep mantle or remained in the upper mantle, are expected to be randomly distributed in the upper mantle in response to the mantle circulation. When transported to beneath ocean ridges, the composite lithologies will melt to produce geochemically variable MORB melts as observed in the ridge segment OH-1 beneath the MAR (see Guo et al., 2021). Melting-induced mixing produced trends in OH-1 MORB lavas; (c) Modeling of melting induced-mixing of a composite mantle source containing varying proportions of petrologically, compositionally and physically distinct two lithologies (i.e., peridotite and pyroxenite) that have co-existed for some length of Earth's history (see Fig. 6a and details in Supplementary). The color-coded numbers on the lines denote the pyroxenite proportions in the melting mantle source. The number (in percent) on the orange triangles represent partial melting degree (5% to 25%) of the pyroxenite. Green diamonds represent partial melting of the peridotite at partial melting degree of 5% to 20%. Subscript N in $[La/Sm]_N$ denotes primitive mantle normalized (Sun and McDonough, 1989).

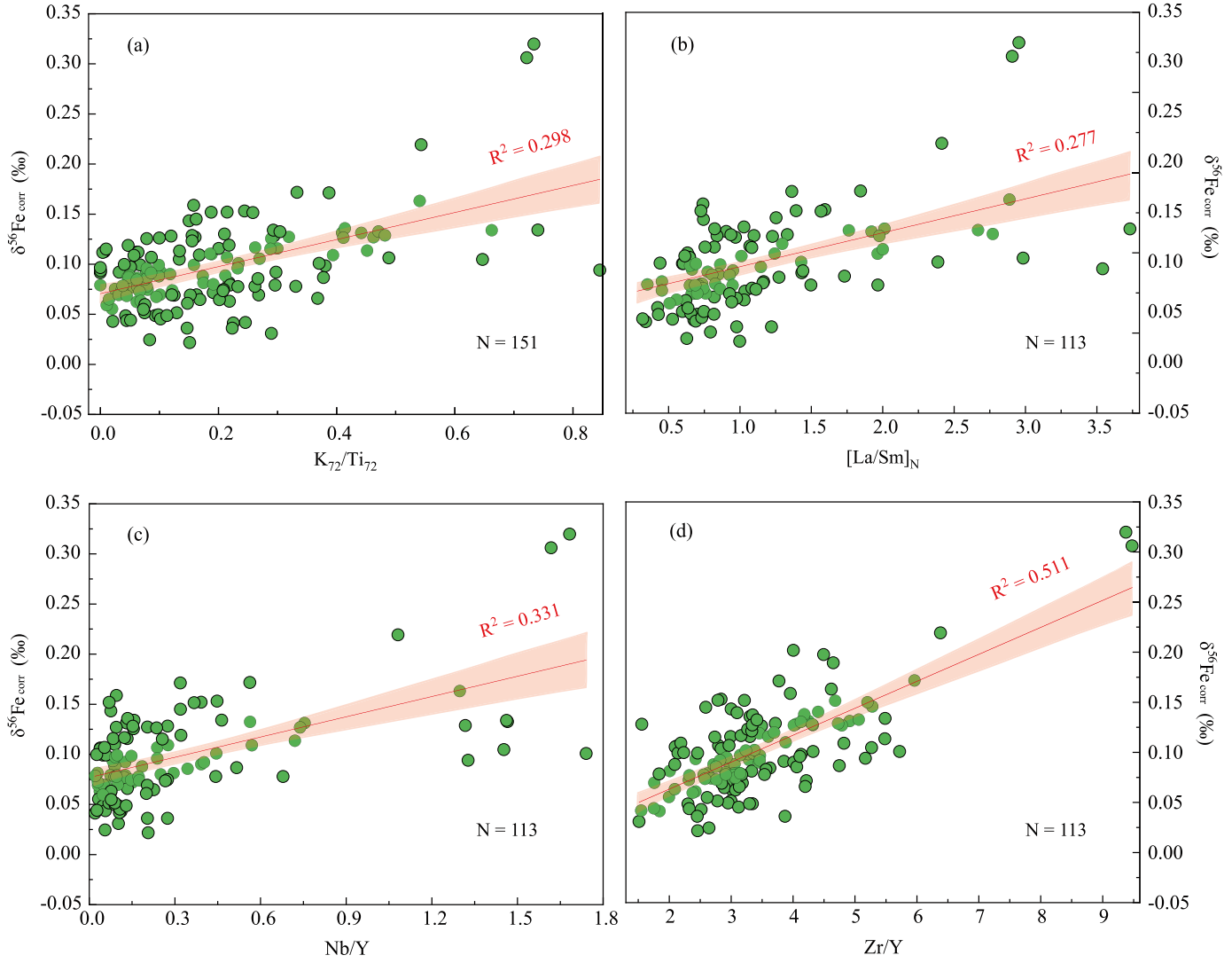

Fig. 7. δ^{56}Fe variations with K_{72}/Ti_{72} (corrected for melt fractionation to Mg# = 0.72), $[La/Sm]_N$, Nb/Y and Zr/Y to show systematic global MORB δ^{56}Fe trends with ratios of more-to-less incompatible elements (data are from this study and literatures Weyer and Ionov, 2007; Nebel et al., 2013; Chen et al., 2019; Sun et al., 2020; Gleeson et al., 2020; Richter et al., 2021).

et al., 2020). That is, there are generally two mantle components in the upper mantle: one is the predominant refractory/depleted peridotite with low δ^{56}Fe and low abundances of incompatible elements; and the other is the metasomatic veins or veinlets with high-δ^{56}Fe, elevated abundances of incompatible elements, most probably in the form of garnet pyroxenite, randomly dispersed in the depleted peridotitic matrix (Fig. 6b). Melting of such a composite upper mantle with varying contributions of lherzolite and pyroxenite can readily produce melts with apparent mixing trends on geochemical diagrams (Fig. 7, also see above Fig. 6c modelling).

4.6. Implications for the origin of the δ^{56}Fe offset between MORB and abyssal peridotite

There is a ~0.1‰ offset in δ^{56}Fe value between averaged global MORB (mantle melts) and abyssal peridotite (e.g., Craddock et al., 2013; Johnson et al., 2020; Chen et al., 2021). Equilibrium Fe isotope fractionation during partial melting may only explain about one third of the δ^{56}Fe offset (i.e., 0.02-0.04‰; Dauphas et al., 2014). While fractional crystallization can elevate δ^{56}Fe of the residual melt because of the removal of liquidus minerals that preferentially concentrating light Fe isotope (e.g., olivine and clinopyroxene; Chen et al., 2019, 2021), most of the reported MORB experienced limited evolution (Fig. S2). Therefore, this offset remains to be better understood. The substantial $\delta^{56}Fe_{corr}$ variation at a given $Mg^{\#}$ (Fig. S2) is consistent with the mantle source Fe isotope heterogeneity. As demonstrated above, most of the MORB samples are "mixtures" resulting from melting-induced mixing of a composite mantle instead of a lithologically simple lherzolite or pyroxenite. Therefore, a direct application of the single-lithology partial melting modeling (Dauphas et al., 2014) is conceptually problematic. To truly understand the origin of such an offset, we conduct a melting-induced mixing modelling of a lithologically composite mantle source, in which we use the average of seven garnet pyroxenites with δ^{56}Fe = +0.131‰ and Fe_2O_3 = 6.121 wt.% (Zhao et al., 2017) to approximate the enriched veins/veinlets of low-F melt metasomatic origin and the thirteen fresh averaged abyssal peridotite with δ^{56}Fe = +0.024‰ and Fe_2O_3 = 7.685 wt.% (Craddock et al., 2013) to approximate the depleted mantle matrix (see Supplementary Table 5). The non-modal partial melting is adopted in this modelling following Williams and Bizimis (2014) and Soderman et al. (2021) (see details in Supplementary materials). Mixing of the peridotite-derived melts and pyroxenite-derived melts at varying proportions produces MORB melts with varying Fe isotope compositions (Fig. 8b and details in Supplementary). Assuming the partial melting degrees of 5% for pyroxenite and

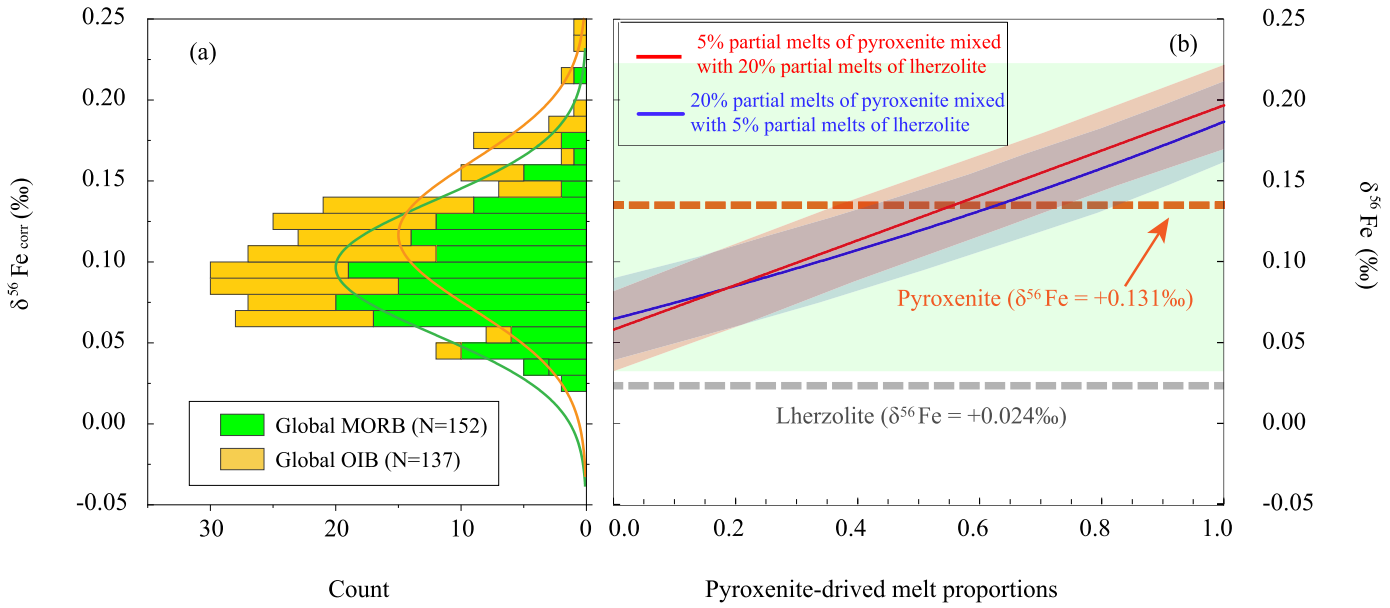

Fig. 8. (a) Histogram of available global MORB and OIB Fe isotope data as in Fig. 2c, but using fractionation-corrected values. Data are of this study and from the literature (Weyer and Ionov, 2007; Teng et al., 2013; Konter et al., 2016; Nebel et al., 2013, 2019; Chen et al., 2019; Peters et al., 2019; Sun et al., 2020; Gleeson et al., 2020; Soderman et al., 2021; Richter et al., 2021; Ruttor et al., 2021; Wang et al., 2021; Shi et al., 2022). The orange and green curves indicate normal distribution of global OIB and MORB, respectively; (b) Modeling of melting induced-mixing of a composite mantle source to illustrate varying contributions of the lherzolite derived-melts and pyroxenite derived-melts can readily produce mixed melts with large Fe isotope compositional variations as displayed in global MORB in (a). The bands represent errors (±SD). The melting induced-mixing model can also help to explain the ~0.1‰ δ^{56}Fe offset between averaged MORB and abyssal peridotite see Chen et al., 2021).

20% for lherzolite, the modelling results indicate varying degrees of mixing between melts from peridotite and pyroxenite can produce the mixed melts with δ^{56}Fe = +0.057 to +0.178‰ (see red line in Fig. 8b). Using different partial melting degrees of 20% for pyroxenite and 5% for lherzolite (see blue line in Fig. 8b) subtly change the ultimately mixed melts Fe isotope compositional variation, but well within the analytical error. In this case, we argue that partial melting-induced mixing model can well explain the offset in δ^{56}Fe values between the abyssal peridotite and the global MORB as well as the δ^{56}Fe variations of the 99% reported global MORB and OIB (Fig. 8a).

5. Conclusions

This study presents Fe isotope compositions of the MORB samples from segment OH-1 of the Mid-Atlantic Ridge (MAR) at ~ 35°N. Our data show a large MORB Fe isotope variation (δ^{56}Fe = +0.03 to +0.18‰) at such a ridge segment scale. The Fe isotope compositions of these MORB correlate well with the abundances and ratios of their incompatible elements and with Sr-Nd-Hf isotopes, successfully verifying the hypothesis that heavy Fe isotope enrichment in the MORB mantle results from the same process of incompatible element enrichment. We explain this process as low-F melt mantle metasomatism taking place at the oceanic LAB in earth's history, and possibly preserved in the pyroxenite veins/veinlets dispersed in the peridotite matrix. Melting of such recycled composite lithologies beneath the present-day sub-ridge produces MORB melts with geochemical correlations as observed at ridge segment OH-1 of the MAR, which we predict to be globally widespread. By compiling the global MORB Fe isotope data, we confirm that the upper mantle is heterogeneous in term of Fe isotopes, and further find the global δ^{56}Fe systematic correlations with the abundances and ratios of their incompatible elements. We suggest that melting-induced mixing of the lithologically heterogeneous upper mantle not only produces the global Fe isotope systematics, but also explains the δ^{56}Fe offset between averaged MORB and abyssal peridotite.

CRediT authorship contribution statement

Pengyuan Guo: Data curation, Formal analysis, Investigation, Methodology, Validation, Writing – original draft. **Yaoling Niu:** Conceptualization, Writing – review & editing. **Shuo Chen:** Investigation, Methodology, Writing – review & editing. **Meng Duan:** Investigation, Methodology. **Pu Sun:** Investigation, Methodology, Writing – review & editing. **Yanhong Chen:** Writing – review & editing. **Hongmei Gong:** Methodology. **Xiaohong Wang:** Methodology.

Declaration of competing interest

The authors declare that they have no known competing financial interests or personal relationships that could have appeared to influence the work reported in this paper.

Data availability

No data was used for the research described in the article.

Acknowledgement

We thank Editor Rosemary Hickey-Vargas for handling this manuscript. We also appreciate Stefan Weyer and an anonymous reviewer for constructive comments and suggestions. This work was co-supported by the National Natural Science Foundation of China (NSFC) (grants 42076048, 91958215, 41776067, 41630968), the NSFC-Shandong Joint Fund for Marine Science Research Centers (U1606401) and the 111 Project (B18048). Dr. Y. He is appreciated for providing the GSB Fe reference material.

Appendix A. Supplementary material

Supplementary material related to this article can be found online at https://doi.org/10.1016/j.epsl.2022.117892.

References

Bebout, G.E., 2013. The role of fluids in terrestrial and extraterrestrial processes. In: Harlov, D., Austrheim, H. (Eds.), Metasomatism and the Chemical Transformation of Rock. Springer-Verlag, Berlin, Heidelberg, pp. 289–349.

Bideau, D., Hékinian, R., Sichler, B., Gracia, E., Bollinger, C., Constantin, M., Guivel, C., 1998. Contrasting volcanictectonic processes during the past 2 Ma on the Mid-Atlantic Ridge: submersible mapping, petrological and magnetic results at lat. 34°52′N and 33°55′N. Mar. Geophys. Res. 20 (5), 425–458.

Canil, D., O'Neill, H.S.C., Pearson, D.G., Rudnick, R.L., McDonough, W.F., Carswell, D.A., 1994. Ferric iron in peridotites and mantle oxidation states. Earth Planet. Sci. Lett. 123 (1–3), 205–220.

Chen, S., Niu, Y., Guo, P., Gong, H., Sun, P., Xue, Q., Duan, M., Wang, X., 2019. Iron isotope fractionation during mid-ocean ridge basalt (MORB) evolution: evidence from lavas on the East Pacific Rise at 10°30′ N and its implications. Geochim. Cosmochim. Acta 267, 227–239.

Chen, S., Wang, X., Niu, Y., Sun, P., Duan, M., Xiao, Y., Xue, Q., 2017. Simple and cost-effective methods for precise analysis of trace element abundances in geological materials with ICP-MS. Sci. Bull. 62, 277–289.

Chen, Y., Niu, Y., Duan, M., Gong, H., Guo, P., 2021. Fractional crystallization causes the iron isotope contrast between mid-ocean ridge basalts and abyssal peridotites. Commun. Earth Environ. 2, 65.

Chen, S., Sun, P., Niu, Y.L., Guo, P.Y., Elliott, T., Hin, R.C., 2022. Molybdenum isotope systematics of lavas from the East Pacific Rise: constraints on the source of enriched mid-ocean ridge basalts. Earth Planet. Sci. Lett. 578, 117283.

Craddock, P.R., Warren, J.M., Dauphas, N., 2013. Abyssal peridotites reveal the near-chondritic Fe isotopic composition of the Earth. Earth Planet. Sci. Lett. 365, 63–76.

Dauphas, N., Craddock, P.R., Asimow, P.D., Bennett, V.C., Nutman, A.P., Ohnenstetter, D., 2009. Iron isotopes may reveal the redox conditions of mantle melting from Archean to Present. Earth Planet. Sci. Lett. 288, 255–267.

Dauphas, N., Roskosz, M., Alp, E.E., Neuville, D.R., Hu, M.Y., Sio, C.K., Tissot, F.L.H., Zhao, J., Tissandier, L., Médard, E., Cordier, C., 2014. Magma redox and structural controls on iron isotope variations in Earth's mantle and crust. Earth Planet. Sci. Lett. 398, 127–140.

Donnelly, K.E., Goldstein, S.L., Langmuir, C.H., Spiegelman, M., 2004. Origin of enriched ocean ridge basalts and implications for mantle dynamics. Earth Planet. Sci. Lett. 226 (3–4), 347–366.

Ferry, J.M., Dipple, G.M., 1991. Fluid flow, mineral reactions, and metasomatism. Geology 19, 211–214.

Gleeson, M.L.M., Gibson, S.A., Williams, H.M., 2020. Novel insights from Fe-isotopes into the lithological heterogeneity of Ocean Island Basalts and plume-influenced MORBs. Earth Planet. Sci. Lett. 535, 116114.

Gong, H., Guo, P.Y., Chen, S., Duan, M., Sun, P., Wang, X., Niu, Y.L., 2020. A re-assessment of nickel-doping method in iron isotope analysis on rock samples using multi-collector inductively coupled plasma mass spectrometry. Acta Geochim. 39, 355–364.

Guo, P.Y., Niu, Y.L., Sun, P., Zhang, J., Chen, S., Duan, M., Gong, H.M., Wang, X., 2021. The nature and origin of the upper mantle heterogeneity beneath the Mid-Atlantic Ridge 33-35°N: a Sr-Nd-Hf isotopic perspective. Geochim. Cosmochim. Acta 307, 72–85.

Guo, P.Y., Niu, Y.L., Sun, P., Ye, L., Liu, J., Zhang, Y., Feng, Y.X., Zhao, J.X., 2016. The origin of Cenozoic basalts from central Inner Mongolia, East China: the consequence of recent mantle metasomatism genetically associated with seismically observed Paleo-Pacific slab in the mantle transition zone. Lithos 240, 104–118.

Halliday, A.N., Lee, D.C., Tommasini, S., Davies, G.R., Paslick, C.R., Fitton, J.G., James, D.E., 1995. Incompatible trace elements in OIB and MORB and source enrichment in the sub-oceanic mantle. Earth Planet. Sci. Lett. 133, 379–395.

He, Y., Meng, X., Ke, S., Wu, H., Zhu, C., Teng, F.-Z., Hoefs, J., Huang, J., Yang, W., Xu, L., Hou, Z., Ren, Z.-Y., Li, S., 2019. A nephelinitic component with unusual δ56Fe in Cenozoic basalts from eastern China and its implications for deep oxygen cycle. Earth Planet. Sci. Lett. 512, 175–183.

He, Y., Ke, S., Teng, F.Z., Wang, T., Wu, H., Lu, Y., Li, S., 2015. High precision iron isotope analysis of geological reference materials by high-resolution MC-ICP-MS. Geostand. Geoanal. Res. 39, 341–356.

Hofmann, A.W., 1997. Mantle geochemistry: the message from oceanic volcanism. Nature 385, 219–229.

Johnson, C.M., Beard, B.L., Weyer, S., 2020. Iron geochemistry: an isotopic perspective. In: Advances in Isotope Geochemistry. Springer International Publishing, pp. 85–148 (Chapter 4).

Konter, J.G., Pietruszka, A.J., Hanan, B.B., Finlayson, V.A., Craddock, P.R., Jackson, M.G., Dauphas, N., 2016. Unusual δ56Fe values in Samoan rejuvenated lavas generated in the mantle. Earth Planet. Sci. Lett. 450, 221–232.

Mahoney, J.J., Sinton, J.M., Kurz, M.D., Macdougall, J.D., Spencer, K.J., Lugmair, G.W., 1994. Isotope and trace element characteristics of a superfast spreading ridge: East Pacific Rise, 13–23°S. Earth Planet. Sci. Lett. 121, 173–193.

McKenzie, D., O'Nions, R.K., 1995. The source regions of oceanic island basalts. J. Petrol. 36, 133–159.

Nebel, O., Arculus, R.J., Sossi, P.A., Jenner, F.E., Whan, T.H.E., 2013. Iron isotopic evidence for convective resurfacing of recycled arc-front mantle beneath back-arc basins. Geophys. Res. Lett. 40, 5849–5853.

Nebel, O., Sossi, P.A., Bénard, A., Arculus, R.J., Yaxley, G.M., Woodhead, J.D., Rhodri Davies, D., Ruttor, S., 2019. Reconciling petrological and isotopic mixing mechanisms in the Pitcairn mantle plume using stable Fe isotopes. Earth Planet. Sci. Lett. 521, 60–67.

Niu, Y.L., Hékinian, R., 2004. Ridge suction drives plume-ridge interactions. In: Hékinian, R., Stoffers, P. (Eds.), Oceanic Hotspots. Springer-Verlag, New York, pp. 285–307 (Chapter 9).

Niu, Y.L., O'Hara, M.J., 2003. Origin of ocean island basalts: a new perspective from petrology, geochemistry, and mineral physics considerations. J. Geophys. Res. 108 (B4).

Niu, Y.L., Green, D.H., 2018. The petrological control on the lithosphere-asthenosphere boundary (LAB) beneath ocean basins. Earth-Sci. Rev. 185, 301–307.

Niu, Y.L., 2014. Geological understanding of plate tectonics: basic concepts, illustrations, examples and new perspectives. Glob. Tecton. Metallog. 10, 23–46.

Niu, Y.L., 1997. Mantle melting and melt extraction processes beneath ocean ridges: evidence from abyssal peridotites. J. Petrol. 38, 1047–1074.

Niu, Y.L., Bideau, D., Hékinian, R., Batiza, R., 2001. Mantle compositional control on the extent of mantle melting, crust production, gravity anomaly, ridge morphology, and ridge segmentation: a case study at the Mid-Atlantic Ridge 33–35°N. Earth Planet. Sci. Lett. 186, 383–399.

Niu, Y.L., Regelous, M., Wendt, J.I., Batiza, R., O'Hara, M.J., 2002. Geochemistry of near-EPR seamounts: importance of source vs. process and the origin of enriched mantle component. Earth Planet. Sci. Lett. 199, 327–345.

Niu, Y.L., Waggoner, G., Sinton, J.M., Mahoney, J.J., 1996. Mantle source heterogeneity and melting processes beneath seafloor spreading centers: the East Pacific Rise 18° - 19°S. J. Geophys. Res. 101, 27711–27733.

O'Neill, H.S.C., Berry, A.J., Mallmann, G., 2018. The oxidation state of iron in Mid-Ocean Ridge Basaltic (MORB) glasses: implications for their petrogenesis and oxygen fugacities. Earth Planet. Sci. Lett. 504, 152–162.

Peters, B.J., Shahar, A., Carlson, R.W., Day, J.M.D., Mock, T.D., 2019. A sulfide perspective on iron isotope fractionation during ocean island basalt petrogenesis. Geochim. Cosmochim. Acta 245, 59–78.

Richter, M., Nebel, O., Schwindinger, M., Nebel-Jacobsen, Y., Dick, H.J.B., 2021. Competing effects of spreading rate, crystal fractionation and source variability on Fe isotope systematics in mid-ocean ridge lavas. Sci. Rep. 11, 4123.

Rouxel, O., Dobbek, N., Ludden, J., Fouquet, Y., 2003. Iron isotope fractionation during oceanic crust alteration. Chem. Geol. 202, 155–182.

Ruttor, S., Nebel, O., Nebel-Yacobsen, Y., Cohen, B.E., Eggins, S., 2021. Alkalinity of ocean island lavas decoupled from enriched source components: a case study from the EM1-PREMA Tasmantid mantle plume. Geochim. Cosmochim. Acta 314, 140–158.

Salters, V.J.M., White, W.M., 1998. Hf isotope constraints on mantle evolution. Chem. Geol. 145, 447–460.

Shi, J.-H., Zeng, G., Chen, L.-H., Hanyu, T., Wang, X.-J., Zhong, Y., Xie, L.-W., Xie, W.-L., 2022. An eclogitic component in the Pitcairn mantle plume: evidence from olivine compositions and Fe isotopes of basalts. Geochim. Cosmochim. Acta 318, 415–427.

Sossi, P.A., O'Neill, H.St.C., 2017. The effect of bonding environment on iron isotope fractionation between minerals at high temperature. Geochim. Cosmochim. Acta 196, 121–143.

Sossi, P.A., Nebel, O., Foden, J., 2016. Iron isotope systematics in planetary reservoirs. Earth Planet. Sci. Lett. 452, 295–308.

Soderman, C.R., Matthews, S., Shorttle, O., Jackson, M.G., Ruttor, S., Nebel, O., Turner, S., Beier, C., Millet, M.-A., Widom, E., Humayun, M., Williams, H.M., 2021. Heavy δ^{57}Fe in ocean island basalts: a non-unique signature of processes and source lithologies in the mantle. Geochim. Cosmochim. Acta 292, 309–332.

Sun, P., Guo, P.Y., Niu, Y.L., 2021. Eastern China continental lithosphere thinning is a consequence of paleo-Pacific subduction: a review and new perspectives. Earth-Sci. Rev. 218, 103680.

Sun, P., Niu, Y., Guo, P., Duan, M., Chen, S., Gong, H., Wang, X., Xiao, Y., 2020. Large iron isotope variation in the eastern Pacific mantle as a consequence of ancient low-degree melt metasomatism. Geochim. Cosmochim. Acta 286, 269–288.

Sun, S.-s, Nesbitt, R.W., Sharaskin, A.Y., 1979. Geochemical characteristics of mid-ocean ridge basalts. Earth Planet. Sci. Lett. 44, 119–138.

Sun, S.-s., Hanson, G.N., 1975. Origin of Ross Island basanitoids and limitations upon the heterogeneity of mantle sources for alkali basalts and nephelinites. Contrib. Mineral. Petrol. 52, 77–106.

Sun, S.-s., McDonough, W.F., 1989. Chemical and isotopic systematics of oceanic basalts: implications for mantle composition and processes. Geol. Soc. Spec. Publ. 42, 313–345.

Teng, F.Z., Dauphas, N., Huang, S., Marty, B., 2013. Iron isotopic systematics of oceanic basalts. Geochim. Cosmochim. Acta 107, 12–26.

Teng, F.Z., Dauphas, N., Helz, R.T., 2008. Iron isotope fractionation during magmatic differentiation in Kilauea Iki lava lake. Science 320 (5883), 1620–1622.

Wang, X.-J., Chen, L.-H., Hanyu, T., Shi, J.-H., Zhong, Y., Kawabata, H., Miyazaki, T., Hirahara, Y., Takahashi, T., Senda, R., Chang, Q., Vaglarov, B.S., Kimura, J.-I., 2021. Linking chemical heterogeneity to lithological heterogeneity of the Samoan mantle plume with Fe-Sr-Nd-Pb Isotopes. J. Geophys. Res. 126, e2021JB022887.

Weyer, S., Ionov, D.A., 2007. Partial melting and melt percolation in the mantle: the message from Fe isotopes. Earth Planet. Sci. Lett. 259, 119–133.

White, W.M., 2015. Probing the Earth's deep interior through geochemistry. Geochem. Perspect. 4 (2), 95–251.
Williams, H.M., Bizimis, M., 2014. Iron isotope tracing of mantle heterogeneity within the source regions of oceanic basalts. Earth Planet. Sci. Lett. 404, 396–407.
Workman, R.K., Hart, S.R., 2005. Major and trace element composition of the depleted MORB mantle (DMM). Earth Planet. Sci. Lett. 231, 53–72.
Zhao, X.M., Cao, H.H., Mi, X., Evans, N.J., Qi, Y.H., Huang, F., Zhang, H.F., 2017. Combined iron and magnesium isotope geochemistry of pyroxenite xenoliths from Hannuoba, North China Craton: implications for mantle metasomatism. Contrib. Mineral. Petrol. 172, 40.
Zindler, A., Staudigel, H., Batiza, R., 1984. Isotope and trace element geochemistry of young Pacific seamounts: implications for the scale of upper mantle heterogeneity. Earth Planet. Sci. Lett. 70, 175–195.